Stem Cell Reports
Article

OPEN ACCESS

The Orphan Nuclear Receptor TLX Represses *Hes1* Expression, Thereby Affecting NOTCH Signaling and Lineage Progression in the Adult SEZ

Inma Luque-Molina,[1,3] Yan Shi,[1,2,3] Yomn Abdullah,[1] Sara Monaco,[1] Gabriele Hölzl-Wenig,[1] Claudia Mandl,[1] and Francesca Ciccolini[1,*]

[1]Department of Neurobiology, Interdisciplinary Center for Neurosciences, University of Heidelberg, Im Neuenheimer Feld 366, 69120 Heidelberg, Germany
[2]Present address: Department of Human Genetics, Radboud University Medical Center, Nijmegen, The Netherlands
[3]Co-first author
*Correspondence: ciccolini@nbio.uni-heidelberg.de
https://doi.org/10.1016/j.stemcr.2019.05.004

SUMMARY

In the adult subependymal zone (SEZ), neural stem cells (NSCs) apically contacting the lateral ventricle on activation generate progenitors proliferating at the niche basal side. We here show that Tailless (TLX) coordinates NSC activation and basal progenitor proliferation by repressing the NOTCH effector *Hes1*. Consistent with this, besides quiescence *Hes1* expression also increases on *Tlx* mutation. Since HES1 levels are higher at the apical SEZ, NOTCH activation is increased in $Tlx^{-/-}$ NSCs, but not in surrounding basal progenitors. Underscoring the causative relationship between higher HES1/NOTCH and increased quiescence, downregulation of *Hes1* only in mutant NSCs normalizes NOTCH activation and resumes proliferation and neurogenesis not only in NSCs, but especially in basal progenitors. Since pharmacological blockade of NOTCH signaling also promotes proliferation of basal progenitors, we conclude that TLX, by repressing *Hes1* expression, counteracts quiescence and NOTCH activation in NSCs, thereby relieving NOTCH-mediated lateral inhibition of proliferation in basal progenitors.

INTRODUCTION

The subependymal zone (SEZ) is the main germinal niche in the brain of adult rodents where neural stem cells (NSCs) generate new olfactory bulb interneurons throughout adulthood. As in most adult tissue, NSCs undergo quiescence in the adult brain, which is essential to prevent their exhaustion. On activation, quiescent NSCs re-enter the cell cycle to self-renew and to generate at the basal side of the niche, rapidly dividing transit-amplifying progenitors (TAPs), which differentiate while proliferating. The maintenance of NSCs during active proliferation as well as quiescence requires the repression of the differentiation program. Key players in this regulation are the mammalian homologs of the *Drosophila* hairy and enhancer of split (*Hes*) 1 and 5 genes. These are transcriptional repressors counteracting, in neural progenitors, the expression of proneural genes such as the mammalian homolog of *Drosophila achaete scute* (*Mash1*), which promotes differentiation. Among the *Hes* genes expressed in the developing murine brain, *Hes*1 and *Hes*5 are the best studied because they are both targets of canonical NOTCH signaling. Although they exhibit a certain degree of functional homology (Hatakeyama et al., 2004; Ishibashi et al., 1995; Ohtsuka et al., 1999), they are not overlapping. For example, whereas *Hes*5 is mainly under NOTCH control, *Hes*1 expression is regulated also by other signals. Besides preventing differentiation, HES1 is also essential in promoting cell-cycle progression. Indeed, HES1 in embryonic and adult NSCs undergoes temporary oscillations essential for instructing the oscillatory expression of *Mash1*, which has the dual function of promoting precursor proliferation and neuronal differentiation (Andersen et al., 2014; Castro et al., 2011; Imayoshi et al., 2013; Sueda et al., 2019). Underscoring the importance of *Hes1* oscillation, forcing its constant expression leads to cell-cycle exit. However, how *Hes1* expression is regulated in quiescent NSCs is not known.

The orphan nuclear receptor *Tailless* (*Tlx*) mostly functions as a transcriptional repressor (Sun et al., 2007), and it is a critical regulator of adult neurogenesis (Shi et al., 2004). Although *Tlx* is expressed in both cell groups (Li et al., 2012; Obernier et al., 2011), mutation of *Tlx* firstly affects the proliferation of NSCs, but not of TAPs, around the time of birth. Thereafter, in the continuous absence of TLX, NSCs progressively lose the ability of entering the cell cycle with a consequent reduction in the number of TAPs (Obernier et al., 2011). In the adult mutant SEZ, proliferation is very much reduced although NSCs are still present and capable of reactivating on restoration of *Tlx* expression (Li et al., 2012; Obernier et al., 2011). Consistent with its function as transcriptional repressor, we here show that TLX directly inhibits the transcription of *Hes1,* and that *Tlx* mutation leads to increased NOTCH signaling and quiescence in the apical NSCs of $Tlx^{-/-}$ mutant mice. Higher NOTCH activation in apical NSCs also prevents the proliferation of basal progenitors since interference with NOTCH signaling is enough to rescue the proliferation of mutant basal progenitors. Taken together, these findings highlight the role of NOTCH-mediated

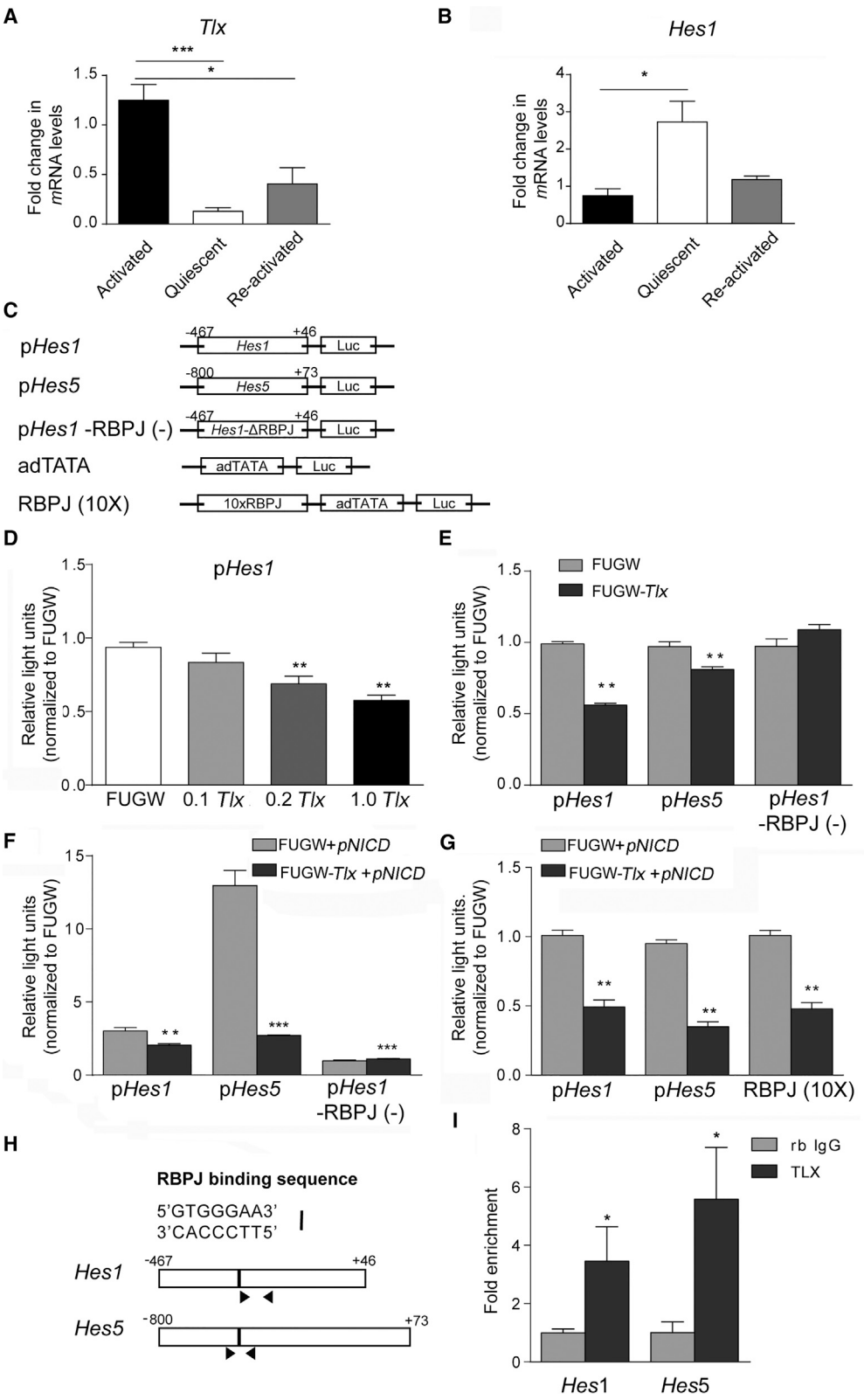

(legend on next page)

interactions in coordinating proliferation between the apical and basal sides of the niche.

RESULTS

TLX Regulates *Hes1* Expression in NSCs

To begin to investigate a possible interaction between *Tlx* and NOTCH signaling in the regulation of NSC quiescence, we firstly analyzed the expression of *Hes1* and *Tlx* in O4ANS cultures of adult NSCs (Pollard et al., 2006) exposed to fibroblast growth factor 2 (FGF2), and either epidermal growth factor (EGF) or BMP4, to induce proliferation and quiescence, respectively (Luque-Molina et al., 2017; Martynoga et al., 2013; Sun et al., 2011). Quantitative mRNA analysis showed a downregulation of *Tlx* (Figure 1A) and an increase in *Hes1* (Figure 1B), but not *Hes5* (data not shown), transcript levels on induction of quiescence. This observation is consistent with our previous finding that *Tlx* is upregulated in activated NSCs (Obernier et al., 2011), and it highlights an inverse correlation between the expression of the two transcriptional regulators during the transition from proliferation to quiescence.

Previous studies have shown that TLX affects the transcription of various genes in neural precursors (Iwahara et al., 2009; Li et al., 2008). Therefore, we next used luciferase assays to test the hypothesis that the orphan nuclear receptor may regulate the activity of the *Hes1* promoter in both HEK cells (Figures 1C–1F) and in neurosphere cultures established from the adult SEZ (Figure 1G). In HEK cells, overexpression of *Tlx* led to a dose-dependent repression of the *Hes1* promoter (Figure 1D) and required the presence of the RBBJ binding site (Figure 1E). A similar effect of TLX on the activity of the *Hes1* promoter was observed also on cotransfection of NOTCH intracellular domain (NICD), to mimic activated NOTCH signaling, in HEK cells (Figure 1F) and in neurosphere cultures (Figure 1G). In both systems TLX similarly repressed an artificial promoter consisting of ten RBPJ sites cloned upstream of the TATA box as well as the activity of the *Hes5* promoter (Figures 1E–1G). However, unlike for the *Hes1* promoter, the inhibitory effect of TLX was much stronger in NICD cotransfected cultures than in parallel cultures transfected only with *Tlx* and the reporter constructs (Figures 1E–1G). The difference was mainly because activation of the *Hes5* promoter was increased by the cotransfection of NICD, which is consistent with previous findings showing that *Hes5* expression is mostly controlled by NOTCH signaling (Basak and Taylor, 2007; de la Pompa et al., 1997; Lutolf et al., 2002). Finally, chromatin immunoprecipitation in neurosphere cultures showed that TLX-specific antibodies, but not control rabbit immunoglobulin G (IgG), were able to immunoprecipitate a complex containing sequences of either promoter (Figures 1H and 1I). Taken together, these data show that TLX regulates transcription from both *Hes* gene promoters by forming a regulatory complex at the RBPJ binding site. They also suggest that modulation of *Hes* gene transcription by the orphan nuclear receptor may contribute to regulate activation and NOTCH signaling in NSCs.

Mutation of *Tlx* Affects NOTCH Signaling in the SEZ

Next, we investigated whether *Tlx* mutation affects NOTCH signaling in postnatal NSCs by measuring the expression of NOTCH-relevant genes in sorted wild-type (WT) neural precursors and their counterpart isolated

Figure 1. TLX Regulates *Hes1* and *Hes5* Genes by Interacting with Their Promoters

(A and B) Quantitative analysis of *Tlx* (A) and *Hes1* (B) transcript levels in the cell line O4ANS, cultured under the growth factor conditions of activation, reactivation (exogenous EGF and FGF2), or quiescence (exogenous BMP4 and FGF2) as indicated. Data are normalized to O4ANS cells in activation state.

(C) Schematic illustration of the plasmids used for the luciferase assay: p*Hes1*, the plasmid construct coding the luciferase gene under the control of the murine *Hes1* promoter (from nucleotide −467 to nucleotide +46); p*Hes1*-RBPJ (−), the plasmid on deletion of the RBPJ binding site from p*Hes1*; p*Hes5*, the plasmid construct coding the luciferase gene under the control of the murine *Hes5* promoter (from nucleotide −800 until nucleotide +73); adTATA, the plasmid expressing the luciferase gene under the control of an adTATA box; RBPJ (10×), the plasmid expressing the luciferase gene under the control of ten copies of the RBPJ binding site (pRBPJ-AdTATA-Luc or p10XCBF1-luc).

(D–G) Quantitative analyses of luciferase activity on transfection of HEK293 cells (D–F) and neurosphere cultures (G) with reporter plasmids p*Hes1*, p*Hes5*, p*Hes1*-RBPJ, and RBPJ (10×), and with either a control plasmid (FUGW) or a plasmid overexpressing *Tlx*, or with a plasmid overexpressing *Tlx* and the activated NOTCH1 receptor intracellular domain (NICD) (F and G).

(H) Scheme illustrating the regions in the *Hes1* and *Hes5* promoters amplified by the primers (arrows) in the chromatin immunoprecipitation assay (ChIP). The vertical bar represents the position of the RBPJ binding sequence.

(I) Quantitative analysis of the ChIP assay showing an enrichment of the amplified fragments of the *Hes1* and *Hes5* promoter on immunoprecipitation with TLX antibodies. RNA expression data are shown as the mean of relative quantification (RQ) from ddCT ± SEM, $n \geq 4$ (A and B). Luciferase and ChIP data are presented as means ± SEM normalized to control, $n \geq 4$.

$^{*}p \leq 0.05$, $^{**}p \leq 0.01$, $^{***}p \leq 0.001$.

from *Tlx*$^{-/-}$ mutant mice (Roy et al., 2004). Using this mouse model, we have previously shown, from birth onward, a progressive loss of proliferating NSCs and TAPs in the SEZ of *Tlx*$^{-/-}$ mice and consequent ventricle enlargement (Obernier et al., 2011). In this earlier study, we also reported that the mutation firstly affects the ability of NSCs to enter the cell cycle, underscored by the fact that defective proliferation and upregulation of negative cell-cycle regulators were both observed in mutant activated NSCs but not in the TAP counterpart. Therefore, we firstly analyzed the expression of *Hes1* and *Hes5*, and of *Mash1*, which is negatively regulated by NOTCH signaling, in activated NSCs and TAPs obtained from WT and *Tlx*$^{-/-}$ neonatal mice (Figures 2A–2C). As described previously (Carrillo-Garcia et al., 2010; Cesetti et al., 2011; Khatri et al., 2014), activated NSCs and TAPs were isolated by flow cytometry based on high levels of EGFR (E^h) expression and differential Prominin1 (P) immunoreactivity as P^+/E^h and P^-/E^h cells, respectively (Figure S1A). Supporting our hypothesis that *Tlx* mutation affects NOTCH signaling in NSCs, we found a change in gene expression in mutant P^+/E^h-activated NSCs but not in P^-/E^h TAPs (Figures 2A–2C). Compared with the WT counterpart, *Hes1* transcript levels (Figure 2A) were increased, whereas those of *Mash1* (Figure 2C) were decreased in mutant NSCs. In contrast to *Hes1*, the expression of *Hes5* was also downregulated (Figure 2B), which may be due to a compensatory interaction between the two *Hes* genes (Hatakeyama et al., 2004; Ohtsuka et al., 1999). We next investigated transcript levels of NOTCH-relevant genes in the remaining populations of the neonatal SEZ (Figures 2D and 2E), i.e., P^+E^l cells (Figure 2D), which include ependymal cells and a small fraction of primitive NSCs and P^-E^l cells (Figure 2E), representing neuroblasts and most of the SEZ cells (Carrillo-Garcia et al., 2010; Cesetti et al., 2011; Khatri et al., 2014). We have previously found that perinatal NSCs originating from the ventral germinal zone are firstly affected in *Tlx*$^{-/-}$ mice (Obernier et al., 2011), which suggests a regional regulation. Therefore, we next separately dissected the ventral and dorsal portions of the SEZ, as illustrated in Figure 2D. Quantitative transcript analysis in the two cell groups highlighted several abnormalities in both populations of mutant precursors. Independent of the subregion and of the cell group, *Hes1* was consistently upregulated in mutant cells (Figures 2D and 2E). Levels of *Notch3* but not *Notch1* transcripts were also increased in mutant P^+E^l cells originating from both the ventral and dorsal SEZ (Figure 2D), whereas a similar overexpression was only detected in ventral but not in dorsal P^-E^l cells (Figure 2E). However, within this cell group, transcripts for *Hes5* and the NOTCH ligand *Delta like (Dll)1* showed a significant increase in cells isolated from the ventral and dorsal SEZ, respectively (Figure 2E). In addition, in the SEZ of adult mutant mice, EGFR (Figures S1A and S1B) and MASH1 (Figures S1C and S1D) proteins were both downregulated, suggesting that *Tlx* mutation affects NOTCH signaling also at this age. Therefore, next we investigated *Hes1* expression and NOTCH signaling in the adult SEZ using antibodies to HES1 and NICD. Since the mutant SEZ, compared with the WT counterpart, displays a drastic reduction in the number of basal, but not apical, cells (Figures 3A and 3B), we quantified levels of immunoreactivity separately in the apical and basal subregions of the SEZ. Independent of the genotype, HES1 immunoreactivity measured by fluorescence intensity, was increased at the apical side of the SEZ (Figures 3C and 3D). Moreover, consistent with our finding that TLX represses *Hes1* expression, in both subregions HES1 immunoreactivity was higher in the SEZ of *Tlx*$^{-/-}$ mice than in the WT counterpart (Figure 3D). Reflecting the differential expression levels between the genotypes and the two subregions of the SEZ, more NICD immunopositive ($NICD^+$) cells were found in the apical SEZ of *Tlx*$^{-/-}$ mice, than in the respective basal subregion and in the apical SEZ of WT mice (Figures 3E and 3F). Taken together, these data confirm our findings in the neonatal mice. To better characterize the extra $NICD^+$ cells present in the apical mutant niche, we next dissected the whole adult SEZ of WT and *Tlx*$^{-/-}$ mice to sort P^+E^l and P^-E^l cells. Adult activated P^+E^h NSCs and P^-E^h TAPs were not investigated because both populations are extremely rare in the mutant niche (see Figures S1A and S1B). Sorted P^+E^l and P^-E^l cells were briefly left to adhere onto coverslips before being fixed and processed for immunostaining (Figure 4A). The genotype did not affect NICD immunoreactivity in P^+E^l cells (Figure 4B). In contrast, a higher proportion of *Tlx*$^{-/-}$ P^-E^l cells were $NICD^+$ than the WT counterpart (Figure 4C). Moreover, the extra $NICD^+$ P^-E^l cells in the mutant SEZ were also immunopositive for the glial fibrillary acidic protein (GFAP), but not for Doublecortin (DCX), Nestin, or LeX-SSEA1 (Figures 4D and 4E). Since Prominin-1 is found in apical cells, this result was in apparent contradiction with our previous finding that NICD immunoreactivity is increased in the apical side of the mutant SEZ. We therefore next labeled the apical membrane of the mutant SEZ with DiI before cell dissociation and sorting of P^- cells. Quantitative analysis revealed a 2-fold increase in the percentage of $NICD^+$ cells in DiI-labeled (D^+) P^- cells than in the (D^-) counterpart (D^+P^-: 2.10 ± 0.06; $p < 0.05$), whereas no difference in NICD immunoreactivity was observed between D^-P^+ and D^+P^+ cells (data not shown). Taken together, these data suggest that loss of *Tlx* expression leads to increased HES1 in the SEZ, increased NOTCH activation in the apical side of the niche and a general deregulation of the expression of genes associated with NOTCH signaling.

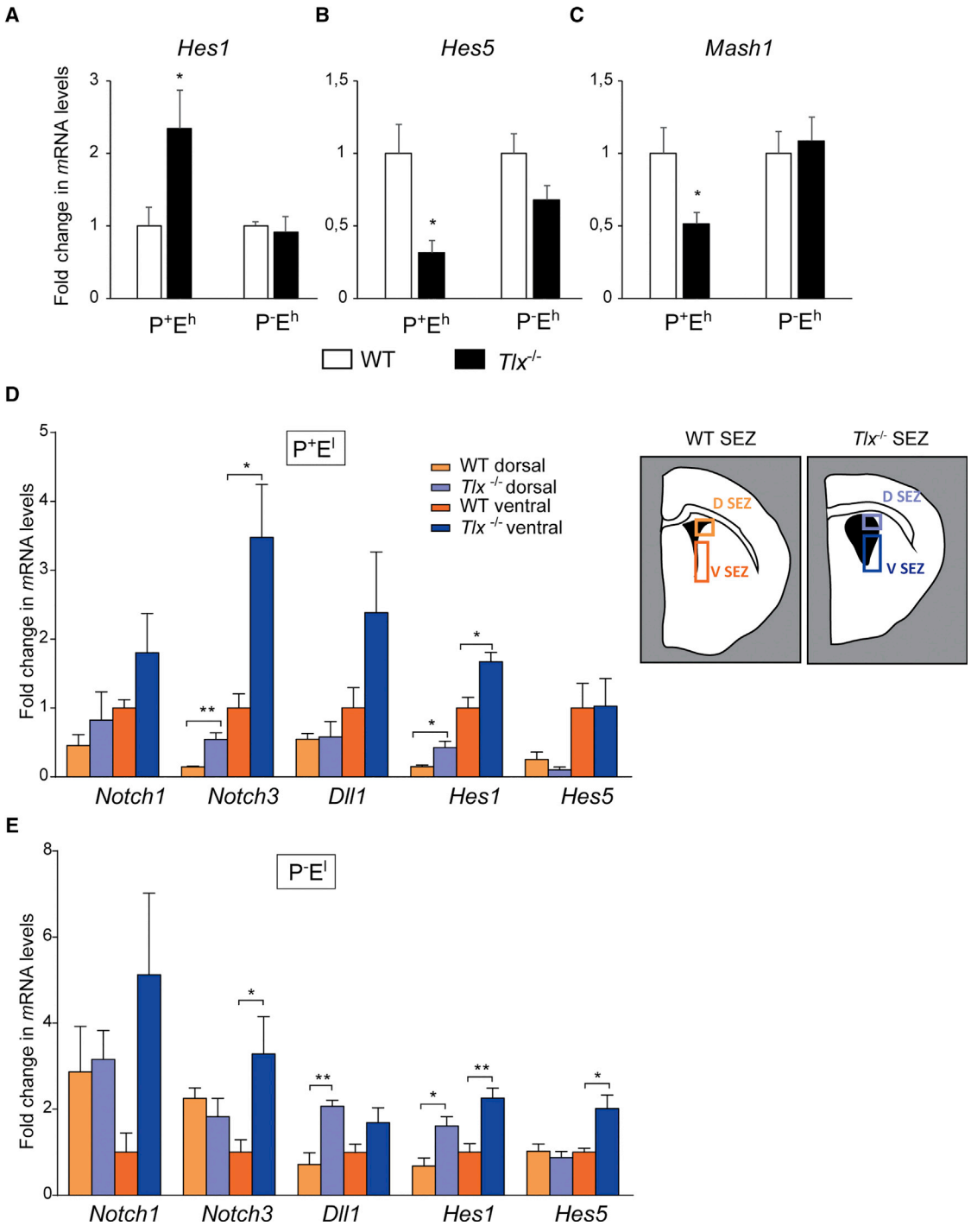

Figure 2. Mutation of *Tlx* Affects NOTCH Signaling Genes in SEZ

Quantitative analysis of transcripts in cells isolated by FACS from the subependymal zone (SEZ) of WT and $Tlx^{-/-}$ mice at postnatal day (P) 7, based on high (E^h) or low (E^l) EGFR levels and differential levels of Prominin1 (P) expression.

(A–C) Quantitative analysis of *Hes1* (A), *Hes5* (B), and *Mash1* (C) transcripts in P^+E^h activated NSCs and P^-E^h TAPs.

(D and E) Dorsal-ventral quantitative gene expression analysis of NOTCH signaling associated genes in P^+E^l (D) and P^-E^l (E) cells. Fold changes are normalized to WT P^-E^- in (A–C) and to WT ventral P^+E^l (D) and WT ventral P^-E^l (E). RNA expression is shown as the mean of RQ from ddCT ±SEM, $n \geq 6$.

*$p \leq 0.05$, **$p \leq 0.01$, ***$p \leq 0.001$. TAPs, transit-amplifying progenitors; SEZ, subependymal zone; D, dorsal; V, ventral.

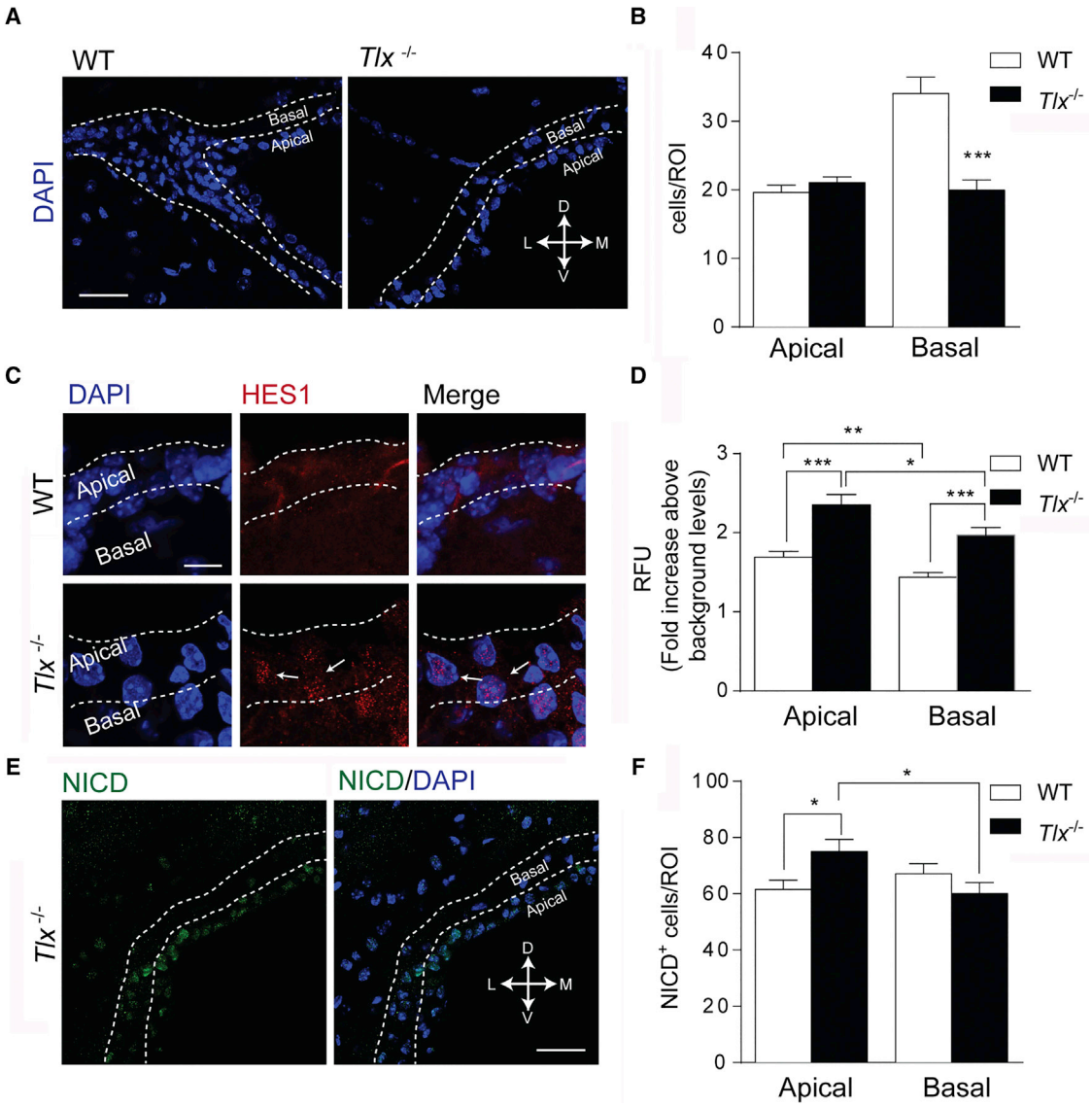

Figure 3. Mutation of *Tlx* Leads to Fewer Cells in the Basal SEZ and Affects *Hes1* Expression and NOTCH Activation

Analysis of the cytoarchitecture (A and B), HES1 levels (C and D), and NOTCH activation (E and F) in the apical and basal SEZ of WT and $Tlx^{-/-}$ mice, as indicated. (A, C, and E) Confocal microphotographs of the SEZ illustrating the different morphology (A) HES1 (red), and (C) NOTCH1 intracellular domain (NICD) immunoreactivity (green) (E) in the SEZ of WT and $Tlx^{-/-}$ adult mice as indicated. DAPI counterstaining of the nuclei is shown in blue. Dashed lines indicate the apical and basal side of the SEZ. Scale bars, 10 μm (C) and 50 μm (A and E). (B, D, and F) Quantitative analyses of the number of cells, as revealed by the nuclei (B), of HES1 immunoreactivity (D), and of the percentage of NICD immunopositive ($NICD^+$) cells (F) in the apical and basal SEZ. Asterisks indicate significant changes between the WT and $Tlx^{-/-}$ population and apical and basal SEZ, as indicated. For HES1 analysis $\geq$30 cells per condition were measured (brightness intensity normalized to background). All data are shown as means ± SEM, n $\geq$ 3. *p $\leq$ 0.05, **p $\leq$ 0.01. ***p $\leq$ 0.001. RFU, relative fluorescence units; M, medial; L, lateral; D, dorsal; V, ventral.

Interference with *Hes1* Expression in the Apical SEZ Normalizes NOTCH Activation and Promotes Proliferation and Lineage Progression in Adult $Tlx^{-/-}$ Mice

Taken together, our data indicate higher HES1 levels in the SEZ of $Tlx^{-/-}$ mice, which promote NOTCH signaling and quiescence in postnatal mutant NSCs. Therefore, we next took advantage of virus-mediated genetic interference to downregulate *Hes1* transcripts in apical cells, including NSCs, by using adeno-associated viral (AAV) particles expressing eGFP, and either a short hairpin to target the *Hes1* mRNAs (AAV-sh*Hes1*) or a scrambled sequence

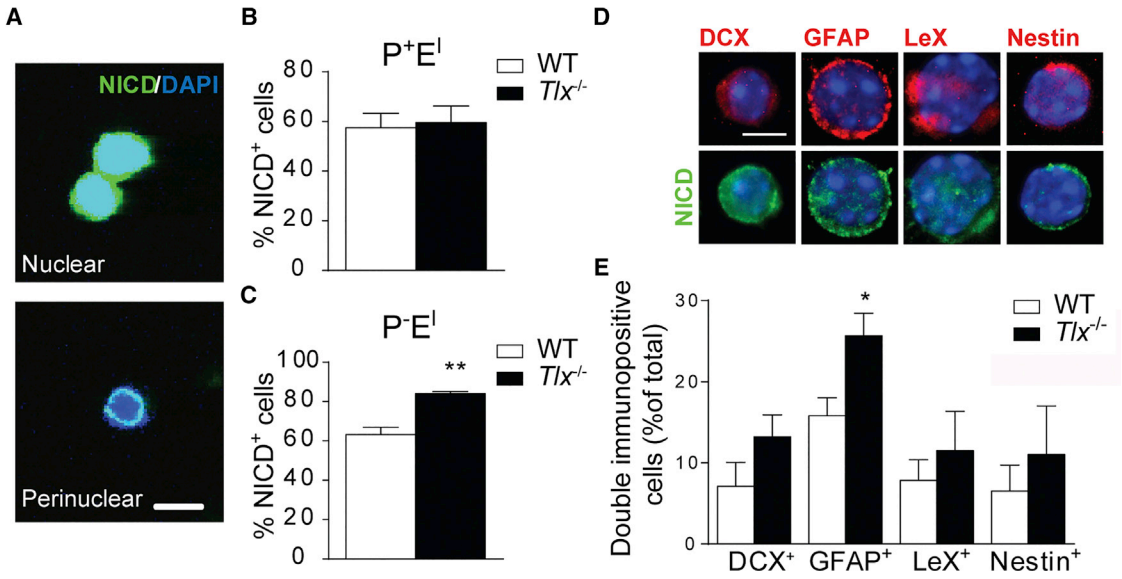

Figure 4. Increased NOTCH Activation in Mutant NSCs Lacking *Tlx* Expression

Antigenic characterization of NICD immunopositive (NICD$^+$) cells. Microphotographs illustrating representative examples of sorted P$^-$E^l cells on single (A) and double immunostaining (D) with NICD (green) alone or in combination with antibodies to the indicated antigens (visualized in red). DAPI counterstaining of the nuclei is shown in blue. Scale bars, 10 μm. Quantitative analysis of the percentage of NICD$^+$ cells in P$^+$E^l and P$^-$E^l on single staining is shown in (B and C), respectively. Quantitative analysis of the double immunostaining illustrated in (D) is shown in (E). DCX, Doublecortin; GFAP, glial fibrillary acid protein; LeX, Lewis X/stage-specific embryonic antigen 1. All data are shown as the means ± SEM, n ≥ 4. *p ≤ 0.05.

(AAV-Scramble). Consistent with previous observations (Kobayashi et al., 2009), preliminary experiments in O4ANS NSC cultures showed that transduction with AAV-sh*Hes1* but not AAV-Scramble, led to downregulation of *Hes1* transcripts (Figure S2A). Moreover, clonal analysis showed that the downregulation of *Hes1* significantly increased the clone-forming ability of dissociated SEZ cells derived from *Tlx*$^{-/-}$ but not of WT mice (data not shown). This is in agreement with the previous observation that other *Hes* genes can compensate *Hes1* ablation in adult NSCs (Sueda et al., 2019). Next we injected the two AAV constructs into the lateral ventricle of *Tlx*$^{-/-}$ adult mice and the animals were sacrificed after 14 days. On immunostaining of coronal sections of the SEZ, we observed that the transduction with AAV-sh*Hes1* led to knockdown of HES1 in the cells of the mutant SEZ, as revealed by the analysis of the intensity of HES1 immunoreactivity in transduced (GFP$^+$) and nontransduced (GFP$^-$) cells (Figures 5A and 5B). This analysis also showed that in AAV-Scramble-injected mice, transduced GFP$^+$ cells displayed higher HES1 levels than the GFP$^-$ counterpart. Since transduced cells were prevalently located in the most apical part of the SEZ, this observation is consistent with our previous finding that disruption of *Tlx* expression leads to increased NOTCH activation at the apical side of the SEZ. Indeed, a similar analysis of NICD showed significantly lower NICD immunoreactivity in GFP$^+$ cells on injection of AAV-sh*Hes1*, but not of AAV-Scramble (Figures 5C and 5D). Downregulation of *Hes1* led also to an increase in the number of cells quantified based on the number of nuclei per region of interest (ROI) (Figure S2B). However, the manipulation did not affect the morphology (Figure S2C), nor the number of GFP-expressing cells (Figure S2D). Instead, compared with the scrambled-injected controls, the number of cells expressing the proliferative antigen Ki67 and the NSC markers Nestin and GFAP were increased in the SEZ of AAV-sh*Hes1*-injected mice (Figures S2E and S2J) in transduced and nontransduced cells, suggesting a non-cell-autonomous effect. Indeed, more cells were cycling in both transduced GFP$^+$ and nontransduced GFP$^-$ cells, not only on *Hes1* downregulation, but the effect was greater in the latter than in the former group (Figures 6A–6C). Likewise, although the number cells immunopositive for GFAP (Figures 6E and 6F) and Nestin (Figures 6H and 6I) displayed a trend to increase in both GFP$^+$ and GFP$^-$ populations of AAV-sh*Hes1*-injected mice, the effect was significant only the latter group (Figures 6F and 6I). Remarkably, independent of the marker analyzed, virtually all the GFP$^-$ immunoreactive cells were localized at the basal side of the niche. Taken together, the easiest explanation for these observations is that the GFP$^-$ immunoreactive cells are derived from a pool of basal progenitors, which are kept quiescent by the high HES1 levels

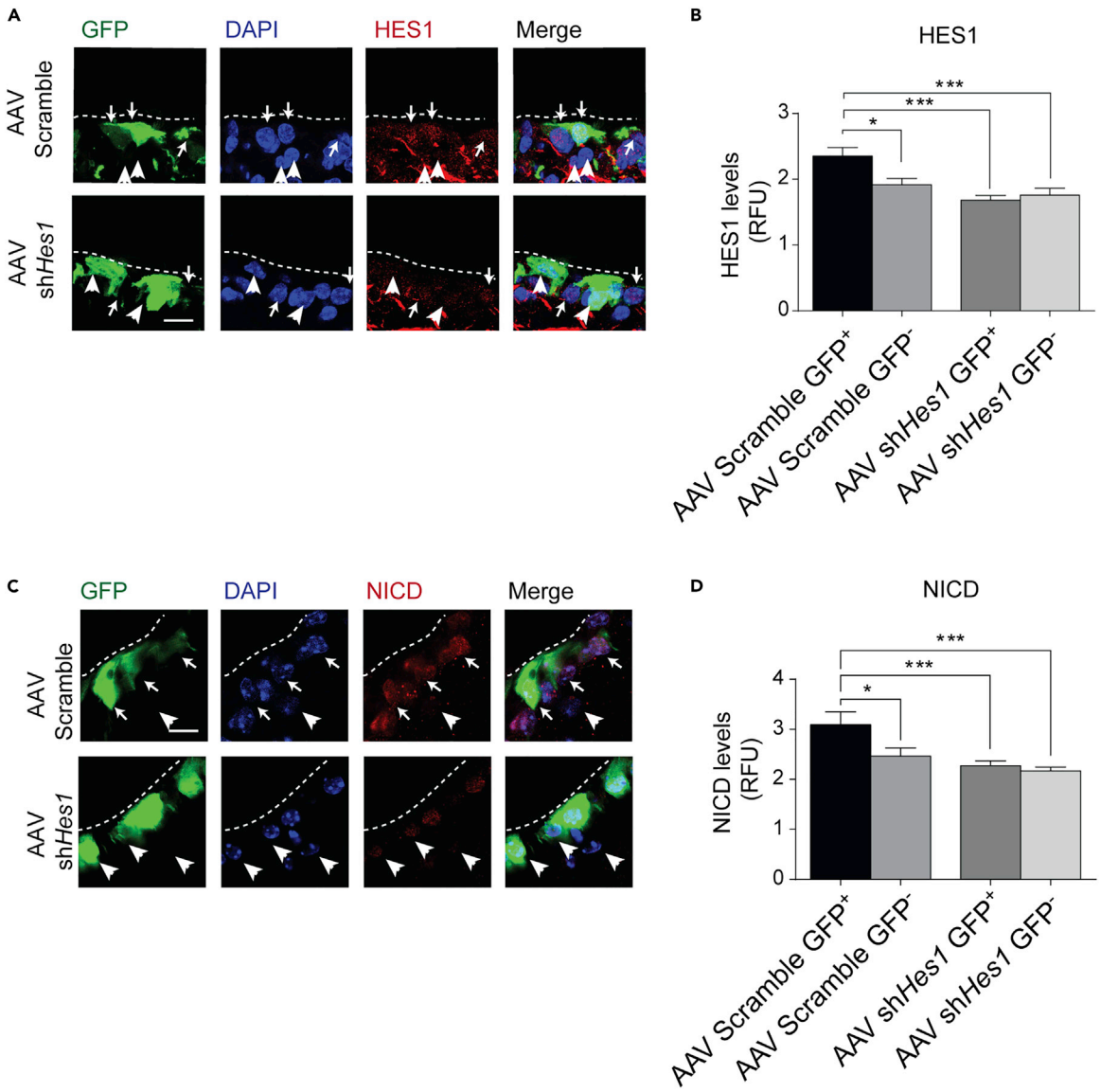

Figure 5. Downregulation of *Hes1* in $Tlx^{-/-}$ Mice Reduces Activation of NOTCH Signaling

Analysis of HES1 (A and B) and NICD expression (C and D) in the SEZ of $Tlx^{-/-}$ adult mice by immunostaining on transduction with adeno-associated viral particles (AAV), containing a construct expressing GFP as reporter gene and either a control scrambled sequence (AAV-Scramble), or a *Hes1* short hairpin (AAV sh*Hes1*). Confocal microphotographs illustrating representative examples of double immunostaining with antibodies to GFP and HES1 (A) or GFP and NOTCH intracellular domain (NICD) (C) and DAPI counterstaining (blue) of the nuclei 14 days after intraventricular injections. Dashed lines in (A and C) indicate the apical side of the SEZ. Quantifications of HES1 and NICD levels (brightness intensity normalized to background) in the cells are shown in (B and D), respectively. Arrows and arrowheads point to cells expressing high and low levels of immunoreactivity, respectively. Data for immunohistochemistry quantification is shown as means ± SEM, n ≥ 30 cells per condition. *p ≤ 0.05, **p ≤ 0.01, ***p ≤ 0.001. Scale bar, 10 μm. RFU, relative fluorescence units.

in the apical mutant niche. We next investigated the effect of transduction with AAV-sh*Hes1* on neurogenesis. Regarding the other protein analyzed above, compared with controls, we found a marked increase in the number of DCX^+ neuroblasts in AAV-sh*Hes1*-transduced mice, the vast majority of which was GFP^- (Figure 6J). Thus, downregulating *Hes1* expression in the mutant SEZ promotes proliferation and neurogenesis in apical and especially basal progenitors, by a cell-autonomous and non-cell-autonomous mechanism, respectively. This shows that overexpression of *Hes1* is a key event leading to impaired NSC proliferation and neurogenesis in mutant mice.

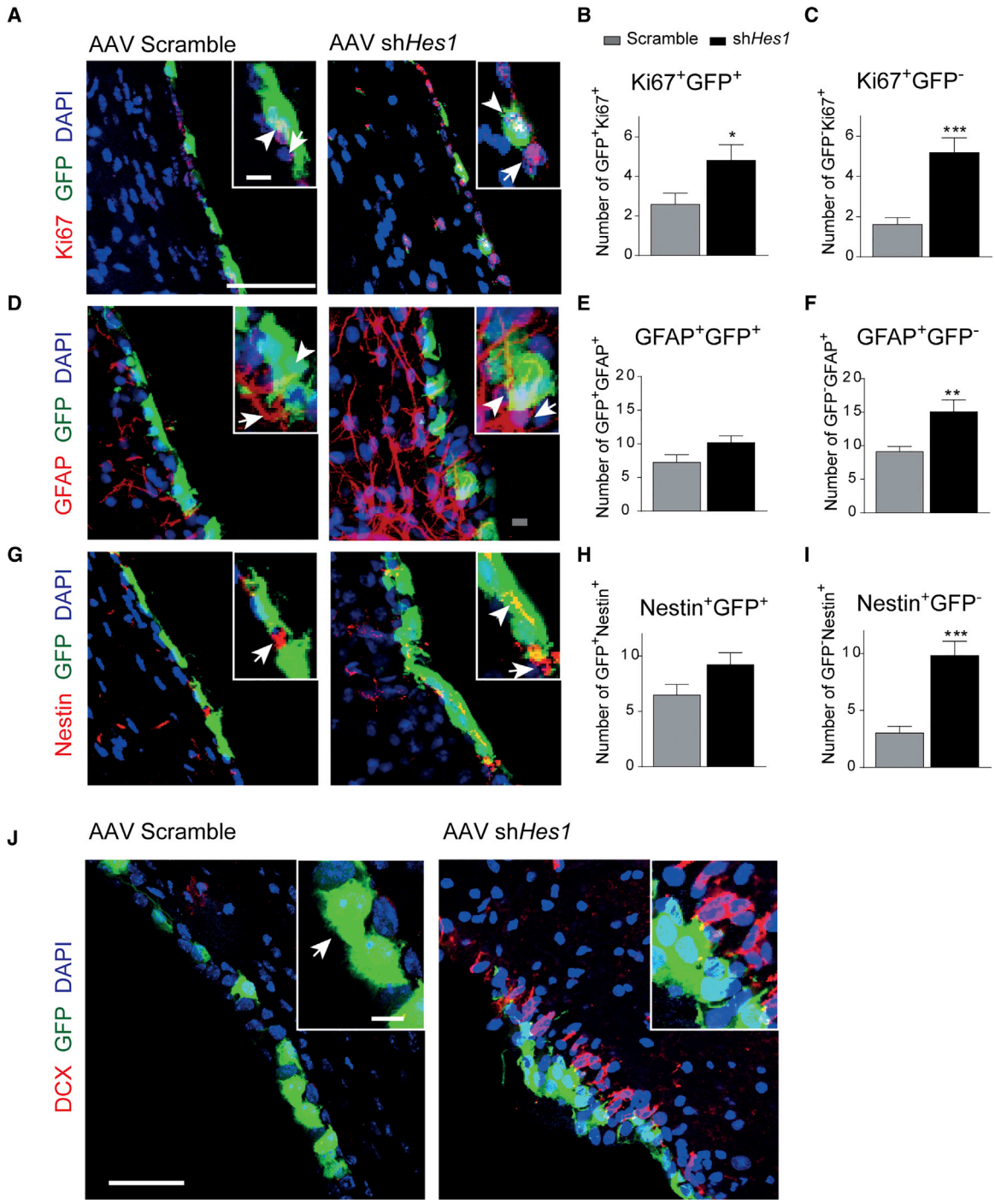

Figure 6. Downregulation of *Hes1* in $Tlx^{-/-}$ Mice Leads to Proliferation and Lineage Progression

Confocal microphotographs illustrating representative examples of double immunostaining of the SEZ of $Tlx^{-/-}$ mice14 days after intraventricular injections with adeno-associated viral particles (AAV), containing a construct expressing GFP as reporter gene and either a control scrambled sequence (AAV-Scramble), or a *Hes1* short hairpin (AAV sh*Hes1*). Coronal sections of the SEZ were processed for immunostaining with antibodies to GFP and Ki67 (A), GFAP (D), Nestin (G), or DCX (J). (B, C, E, F, H, and I) Quantification of the double immunostaining as indicated. Data are shown as mean ± SEM, n ≥ 3. *p ≤ 0.05, **p ≤ 0.01, ***p ≤ 0.001. Scale bars, 50 and 10 μm (magnified). GFAP, glial fibrillary acid protein; DCX, Doublecortin.

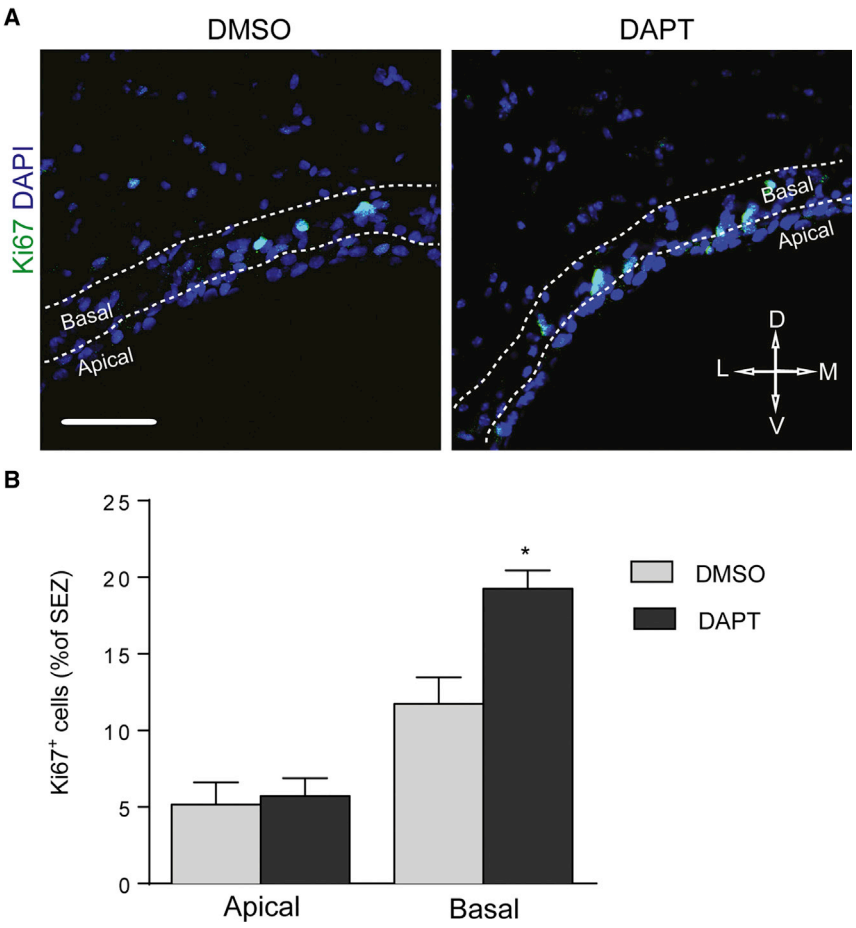

Figure 7. Pharmacological Blockade of NOTCH Signaling Promotes Proliferation of Basal Precursors

(A) Confocal microphotographs illustrating representative examples of Ki67 immunopositive (Ki67$^+$) cells in coronal sections of the SEZ of $Tlx^{-/-}$ adult mice 24 h after intraventricular injection with DMSO or DAPT as indicated. Dashed lines indicate the apical and basal subregion used for the analysis.

(B) Quantification of the Ki67$^+$ cells in apical and basal subregion of SEZ in $Tlx^{-/-}$ mice. All data are shown as mean ± SEM, n ≥ 3. *p ≤ 0.05. Scale bar, 50 μm. M, medial; L, lateral; D, dorsal; V, ventral.

Pharmacological Modulation of NOTCH Signaling Promotes Proliferation of $Tlx^{-/-}$ Precursors

Our previous data show increased HES1 levels and NOTCH signaling in apical NSCs on *Tlx* mutation. They also show that increased apical expression of *Hes1* inhibits proliferation of basal progenitors by a non-cell-autonomous mechanism. Since we have found a general deregulation of the expression of genes associated with NOTCH signaling in the mutant SEZ, we next tested whether the proliferation of mutant basal progenitors was prevented by NOTCH-mediated lateral inhibition. To test this possibility, we blocked endogenous NOTCH signaling by injecting the γ-secretase inhibitor DAPT (N-[N-(3,5-difluorophenacetyl)-L-alanyl]-S-phenylglycine t-butyl ester) (Geling et al., 2002) in the lateral ventricle of $Tlx^{-/-}$ mice. After 24 h, mice were sacrificed and sections of the SEZ were immunostained with Ki67 antibodies to identify cycling cells (Figure 7A). Quantitative analysis of the number of cycling cells in the apical and basal subregions of DMSO- and DAPT-treated $Tlx^{-/-}$ mice showed that, in mutant mice, extra cycling cells were mostly localized in the basal side of the niche (Figure 7B). Thus, in the absence of TLX, increased NOTCH signaling in apical precursors inhibits the proliferation of basal progenitors by NOTCH-mediated lateral inhibition.

DISCUSSION

Our study shows a role for TLX in regulating levels of *Hes1* expression in NSCs. It also demonstrates that the increased *Hes1* expression resulting from *Tlx* disruption affects quiescence and lineage progression by cell-autonomous and non-cell-autonomous mechanisms. In apical mutant NSCs, increased *Hes1* expression promotes NOTCH signaling. This leads to downregulation of the proneural gene *Mash1* in NSCs and increased NOTCH-mediated lateral inhibition of the proliferation of surrounding basal progenitors. Comparative gene expression analysis suggests that NOTCH3 and DLL1 contribute to this interaction, as their transcripts are both upregulated in *Tlx* mutant precursors. Indeed, both molecules have been associated with quiescence in the adult SEZ. For example, niche cells expressing high levels of DLL1 promote NOTCH activation

and NSC quiescence (Kawaguchi et al., 2013). Instead, in the adult SEZ, ablation of *Notch3*, which is expressed predominantly in GFAP immunopositive cells (Basak et al., 2012), leads to a decrease in the number of quiescent NSCs, especially in the lateral and ventral areas of the SEZ (Kawai et al., 2017). NOTCH3 also limits NSC proliferation and lineage progression in the adult zebrafish pallium (Alunni et al., 2013). The downregulation of *Mash1* expression observed in apical NSCs is likely a key to the impaired activation. Indeed, it has been proposed that quiescence, activation, and differentiation of adult NSCs are characterized by absent, intermediate, and high levels of proneural genes expression, which are largely under the control of the *Hes* genes. In particular, the *Hes1* oscillations allow proliferation and lineage progression, whereas its persistent expression leads to cell-cycle exit (Andersen et al., 2014; Baek et al., 2006; Castro et al., 2011; Imayoshi et al., 2013). Consistent with this model, we have previously found that expression of *Mash1* increases with lineage progression from apical NSCs to TAPs (Carrillo-Garcia et al., 2010; Khatri et al., 2014; Obernier et al., 2011). Although multiple factors, including cell-cycle regulators, contribute to control of proneural gene expression levels, oscillation of *Hes1* is critical in the initial phases of cell-cycle entry. Since we found that *Tlx* expression increases as NSCs enter the cell cycle, our data suggest that TLX connects cell-cycle entry and lineage progression. Indeed, downregulation of *Hes1* in $Tlx^{-/-}$ mice not only promoted proliferation but also neurogenesis. This was visible in apical NSCs and especially in basal progenitors, since most cells resuming proliferation and expressing lineage markers were not transduced, and resided in the basal area of the niche. In the developing murine brain, basal progenitors are mostly represented by intermediate progenitors and, to a much lesser extent, outer radial glia (Shitamukai et al., 2011). Since, on downregulation of *Hes1*, many of the basal progenitors in mutant mice express GFAP, they may also represent NSCs that have lost contact with the lateral ventricle, which is in agreement with recent observations (Obernier et al., 2018). These observations underscore that the dynamic NOTCH interaction between apical and basal precursors is key to neurogenesis not only in the developing murine brain (Nelson et al., 2013) but also in the adult niche.

Evidence of a crosstalk between NOTCH signaling and TLX has been reported before. For example, loss of the Tll nematode ortholog nhr-67 affects uterus development in *C. elegans* (VergHese et al., 2011) by disrupting the ability of progenitor cells to undergo NOTCH-dependent asymmetric division, which is necessary to preserve the proliferative potential in one of the daughter cells. Suggestive of a possible interaction between TLX and NOTCH signaling is also the fact that both *Hes1* and *Hes5* are greatly expressed in the retina, the development of which is particularly affected by *Tlx* mutation (Monaghan et al., 1995, 1997). Consistent with our data, upregulated *Hes1* expression was already reported in the SEZ of adult mice lacking TLX (Liu et al., 2008). Whereas on *Tlx* mutation the expression of *Hes1* was consistently upregulated, independently of population, region, and age analyzed, upregulation of *Hes5* was only observed in $P^{-}E^{-}$ originating from the ventral SEZ. Moreover, in neonatal activated NSCs isolated, mutation of *Tlx* led to a decrease in *Hes5* expression. The differential effect of *Tlx* mutation on the expression of the two *Hes* genes may reflect the differential dynamic of binding of RBPJ at the two promoters (Castel et al., 2013). Indeed, we could not detect a classical TLX binding consensus element in the *Hes1* promoter. However, the dependence of TLX repression on the presence of the RBPJ binding site suggests the possibility that TLX may interact with the regulatory complex assembled at this site. Like other orphan nuclear receptors, TLX can bind the AAGTCA, instead of the classical RGNACA consensus although a DNA binding domain located at the amino terminal region of the molecule, both as a monomer and a homodimer (Yu et al., 1994). However, previous studies have already unveiled binding of nuclear receptors in the absence of recognizable binding elements (Cotnoir-White et al., 2011), underscoring the importance of protein-based interactions. Therefore, further studies are necessary to conclusively address the modality of interaction between TLX and the *Hes* promoter.

EXPERIMENTAL PROCEDURES

NSC Line Culture and Experimentation

The line O4ANS of adult murine NSCs was a kind gift from Dr Sprengel, Max Planck Institute of Psychiatry, Molecular Neuroendocrinology, Munich, Germany. These cells were tested for the presence of mycoplasma and cultured as described by Pollard et al. (2006). In normal conditions cells were grown in NS-A medium (Euroclone, Milan, Italy) plus N2 supplement, 2 mM L-glutamine, 100 U/mL penicillin, and 100 μg/mL streptomycin, supplemented with 10 ng/mL FGF2 and 20 ng/mL EGF (PeproTech, Hamburg, Germany). To induce quiescence state, cells were treated with 50 ng/mL BMP4 (R&D Systems, Wiesbaden, Germany) and 20 ng/mL FGF2 (PeproTech) in accordance with the previous published protocol (Luque-Molina et al., 2017). To reactivate them, BMP4 was removed from the medium and cells were cultivated again with 10 ng/mL FGF2 and 20 ng/mL EGF.

Animals and Tissue Dissection

C57BL/6 and $Tlx^{-/-}$ mice experiments were approved by the Regierungspräsidium Karlsruhe and the local authorities at Heidelberg University. Eight-week-old and neonatal mice were sacrificed by CO_2 inhalation followed by cervical dislocation and decapitation, respectively. After this, brains were removed and SEZ was

dissected and dissociated (Ciccolini et al., 2005). Cells from SEZ were processed for flow cytometry. Sorted cells were either isolated for RNA extraction and analysis or plated in at a density of 10^3 cells/mL in culture medium consisting of NS-A complete media supplemented with 2% B27 (Gibco) and 10 ng/mL FGF2 (R&D Systems). For adenovirus infection, cells were plated as described above in the presence of 20 ng/mL EGF (R&D Systems) and transducted with AAV at a density of 1:1,000 of virus suspension in the medium.

For the DiI experiments, SEZ apical surfaces were exposed in the intact brain while DiI (Thermo Fisher Scientific) was added for 3 min. After being washed twice, SEZ were dissected and processed for fluorescence-activated cell sSorting (FACS).

FACS

SEZ cells were incubated at 4°C with anti-Prominin1 antibody conjugated to phycoerythrin (PE) (1:100, Miltenyi Biotec, ref. no. 130-102-210) after 1 h, the antibody was removed and the cells were incubated with EGF-conjugated Alexa 647 (1:1,000, Invitrogen, ref. no. E35351) for 30 min. Afterward, cells were sorted with a FACSAria II (BD Biosciences, Heidelberg, Germany) flow cytometer as described previously (Cesetti et al., 2009; Ciccolini et al., 2005; Khatri et al., 2014)

Analysis of RNA Expression

Cells were sorted directly into RNA lysis buffer (10 μL per 1,000 cells) and total RNA was extracted according to manufacturer's instructions (RNeasy Mini Kit, QIAGEN). Reverse transcription was done using oligo dT primers and M-MLV Reverse Transcriptase (Promega). For quantitative analysis (qPCR), the following TaqMan gene expression assays (Applied Biosystems) were used: *Tlx* (ID: Mm00455855_m1), *Mash1* (ID: Mm04207567_g1), *Hes1* (ID: Mm01342805_m1), *Hes5* (ID: Mm00439311_g1), *Notch1* (ID: Mm00435249_m1), *Notch3* (ID: Mm01345646_m1), *Dll1* (ID: Mm01279269_m1), and *beta Actin (Actb)* (ID: Mm00607939_s1). Cycle threshold values were obtained from the logarithmic phase of amplification plots for the genes of interest and were normalized to the average of *Actb*.

Intraventricular Injections

$Tlx^{-/-}$ mice were anesthetized and intraventricular injected at +1.2 mm anterior-posterior, +0.8 mm medium-lateral, and −2.5 mm dorsal-ventral from bregma. They were injected with either 1 μL DMSO or 1 μL (10 mM) of the γ-secretase DAPT or with 1 μL of AAV containing a plasmid-encoding small hairpin RNA for *Hes1* knockdown under the U6 promoter or a scramble sequence as control. The sequence for *Hes1* knockdown was 5′-GTAGAGAGCTGTATTAAGTGA-3′ (Kobayashi et al., 2009). The humanized recombinant GFP contained in the AAV constructs is driven by chicken β actin promoter and followed by woodchuck hepatitis virus postranscriptional regulatory element and bovine growth hormone (*bGH*) polyA signal.

Immunofluorescence

Perfusion was performed in mice with PBS followed by 4% formaldehyde (PFA) in PBS. Sorted cells were kept in Matrigel-coated chamber slides for 2 h and then fixed in 4% PFA. Coronal sections from the brains and fixed cells were treated with 0.5% NP-40 followed by a blocking solution (5% fetal calf serum in PBS). Thereafter, they were incubated at 4°C with the primary antibodies overnight. These were: TLX rabbit IgG (1:100, LifeSpan bioScience, ref. no. LS-B4564), HES1 mouse IgG2b (1:100, Santa Cruz, ref. no. Sc-166410), MASH1 mouse IgG (1:200, BD Pharmingen, ref. no. 556604), Ki67 rabbit IgG (1:500, Abcam, ref. no. 16667), NICD1 rabbit IgG (1:400, Abcam, ref. no. ab8925), GFAP mouse IgG1 (1:1,000, Sigma, ref. no. G3893), DCX goat IgG (1:100, Santa Cruz, ref. no. sc-390645), Nestin mouse IgG1 (1:100, Sigma, ref. no. 556309), LeX SSEA1 mouse IgM (1:30, Hybridoma Bank, Iowa, IA ref. no. MC-480).

Most of the pictures were taken with a Nikon A1R confocal microscope, using the Nikon Imaging Center facility from the University of Heidelberg.

Luciferase and Chromatin Immunoprecipitation Assay

For luciferase assay in HEK293FT cells, 4×10^4 cells were plated before the transfection. SEZ cells were obtained from neurospheres cultures isolated from P7 mice. These neurospheres were dissociated, and 5×10^5 cells were transfected by a 4D-Nucleofector (Lonza). Forty-eight hours after the transfection, the luminescence was measured according to manufacturer instructions (Dual-Glo Luciferase Assay System, Promega). The ratio of firefly to Renilla luminescence was calculated for each well and then normalized to control (FUGW). Every sample was replicated with three repetitions. Plasmids used for the transfection: pGL4.83[hRlucP/EF1/Puro] (Sepp et al., 2012), pHes1(467)-luc (Addgene, plasmid no. 41723) (Nishimura et al., 1998), pHes1-RBPJ(−)-Luc (Addgene, plasmid no. 43805) (Nishimura et al., 1998), pHes5-Luc (Addgene, plasmid no. 41724) (Nishimura et al., 1998), pRBPJ-AdTATA-Luc or p10XCBF1-luc (McKenzie et al., 2006), pAdTATA-Luc (McKenzie et al., 2006), pFUGW (Addgene, plasmid no. 14883) (Lois et al., 2002) or pFUGW-*Tlx* (Obernier et al., 2011), and pCAGGS-mNICD1 (Addgene, plasmid no. 26891) (Dang et al., 2006).

For the chromatin immunoprecipitation assay (ChIP) assay, neurospheres from adult WT SEZ were used. These neurospheres were dissociated and 1×10^6 cells were used for transfection. Cells were transfected with 5 μg pFUGW-Tlx and 4 μg pCAGGS-NICD1 by 4D-Nucleofector, and cultured for 48 h before being fixed. The sample was crosslinked by adding paraformaldehyde (final concentration 1%) and quenched by adding glycine 1.25 M for 5 min. Cells were then centrifuged, and cell suspensions were treated with protease inhibitor cocktail II (Roche). The DNA of cell suspension was sheared into 200–1,000 bp by sonicating for 5 min with 30 s off between 30-s pulses. Samples were incubated with Tlx rabbit IgG (LifeSpan BioSciences, 1:100) or normal rabbit IgG (for control) at 4°C for 1 h before adding Protein G beads (Dynabeads Protein G, Life Technologies) for overnight incubation. Afterward the protein/DNA complex was eluted from the beads and DNA was purified (QIAquick PCR Purification Kit, QIAGEN) to perform a qPCR to analyze the enrichment of DNA/protein complexes. Primers used: Sense: 5′-CTGGGCTTTGCTTAGTTT-3′, Antisense 5′-TTTAC CTTGTTCCCTCCT-3′ for *Hes1*, and Sense 5′-GCACGCTAAATT GCCTGTGA-3′, Antisense 5′-CCCGGGATGCTAATGAGGAC-3′ for *Hes5*. The protocol was modified from Magna ChiP A kit (Millipore).

Quantification and Statistical Analysis

Immunopositive cells were counted in relation to the total cell number showed by 4DAPI with a systematic random procedure. In analysis of ROI, cells were counted within a fixed rectangular area (15,000 μm^2) aligned with the longest side along the apical side of the SEZ. For quantification of the protein levels in the nuclei, all slices processed for immunohistochemistry were incubated with the same antibody mix. After mounting on coverslip, images of confocal sections were taken across whole nuclei at a distance of 1 μm with a Leica SP8 confocal microscope using a HyD detector, which allows photon quantification per pixel. The fluorescence intensity was then measured on Z projection using ImageJ and normalized to the background. For this analysis, ≥ 30 cells per condition were measured. Quantitative data are showed as the mean ± SEM of at least three independent experiments for each analysis. The power of each experiment was calculated using the statistical software G-Power (Faul et al., 2007). Statistical test (Student's t test and Welch's t test) were calculated using a statistical package (GraphPad Prism). Calculated p values are indicated as: $*p \leq 0.05$, $**p \leq 0.01$, $***p \leq 0.001$.

SUPPLEMENTAL INFORMATION

Supplemental Information can be found online at https://doi.org/10.1016/j.stemcr.2019.05.004.

AUTHOR CONTRIBUTIONS

I.L.-M. collected and analyzed the data and wrote the paper. C.M. and G.H.-W. collected the data. Y.S., Y.A., and S.M. collected and analyzed the data. F.C. conceived and designed the overall data, interpreted the results, and wrote the paper.

ACKNOWLEDGMENTS

Y. S. was supported by a grant from the program Adulte Stammzellen II of the Baden-Württemberg Stiftung. L.M. and S.M were supported by grants CI 43/4-1 and CI 43/11-1 of the Deutsche Forschungsgemeinschaft. *Tlx*$^{-/-}$ mice were generously made available by Dr. Paula Monaghan-Nichols, University of Pittsburgh, Pittsburgh, Pennsylvania, USA.

Received: October 8, 2018
Revised: May 6, 2019
Accepted: May 6, 2019
Published: June 6, 2019

REFERENCES

Alunni, A., Krecsmarik, M., Bosco, A., Galant, S., Pan, L., Moens, C.B., and Bally-Cuif, L. (2013). NOTCH3 signaling gates cell cycle entry and limits neural stem cell amplification in the adult pallium. Development *140*, 3335–3347.

Andersen, J., Urban, N., Achimastou, A., Ito, A., Simic, M., Ullom, K., Martynoga, B., Lebel, M., Goritz, C., Frisen, J., et al. (2014). A transcriptional mechanism integrating inputs from extracellular signals to activate hippocampal stem cells. Neuron *83*, 1085–1097.

Baek, J.H., Hatakeyama, J., Sakamoto, S., Ohtsuka, T., and Kageyama, R. (2006). Persistent and high levels of Hes1 expression regulate boundary formation in the developing central nervous system. Development *133*, 2467–2476.

Basak, O., Giachino, C., Fiorini, E., Macdonald, H.R., and Taylor, V. (2012). Neurogenic subventricular zone stem/progenitor cells are NOTCH1-dependent in their active but not quiescent state. J. Neurosci. *32*, 5654–5666.

Basak, O., and Taylor, V. (2007). Identification of self-replicating multipotent progenitors in the embryonic nervous system by high NOTCH activity and Hes5 expression. Eur. J. Neurosci. *25*, 1006–1022.

Carrillo-Garcia, C., Suh, Y., Obernier, K., Holzl-Wenig, G., Mandl, C., and Ciccolini, F. (2010). Multipotent precursors in the anterior and hippocampal subventricular zone display similar transcription factor signatures but their proliferation and maintenance are differentially regulated. Mol. Cell. Neurosci. *44*, 318–329.

Castel, D., Mourikis, P., Bartels, S.J., Brinkman, A.B., Tajbakhsh, S., and Stunnenberg, H.G. (2013). Dynamic binding of RBPJ is determined by NOTCH signaling status. Genes Dev. *27*, 1059–1071.

Castro, D.S., Martynoga, B., Parras, C., Ramesh, V., Pacary, E., Johnston, C., Drechsel, D., Lebel-Potter, M., Garcia, L.G., Hunt, C., et al. (2011). A novel function of the proneural factor Ascl1 in progenitor proliferation identified by genome-wide characterization of its targets. Genes Dev. *25*, 930–945.

Cesetti, T., Fila, T., Obernier, K., Bengtson, C.P., Li, Y., Mandl, C., Holzl-Wenig, G., and Ciccolini, F. (2011). GABAA receptor signaling induces osmotic swelling and cell cycle activation of neonatal prominin+ precursors. Stem Cells *29*, 307–319.

Cesetti, T., Obernier, K., Bengtson, C.P., Fila, T., Mandl, C., Holzl-Wenig, G., Worner, K., Eckstein, V., and Ciccolini, F. (2009). Analysis of stem cell lineage progression in the neonatal subventricular zone identifies EGFR+/NG2- cells as transit-amplifying precursors. Stem Cells *27*, 1443–1454.

Ciccolini, F., Mandl, C., Holzl-Wenig, G., Kehlenbach, A., and Hellwig, A. (2005). Prospective isolation of late development multipotent precursors whose migration is promoted by EGFR. Dev. Biol. *284*, 112–125.

Cotnoir-White, D., Laperriere, D., and Mader, S. (2011). Evolution of the repertoire of nuclear receptor binding sites in genomes. Mol. Cell. Endocrinol. *334*, 76–82.

Dang, L., Yoon, K., Wang, M., and Gaiano, N. (2006). NOTCH3 signaling promotes radial glial/progenitor character in the mammalian telencephalon. Dev. Neurosci. *28*, 58–69.

de la Pompa, J.L., Wakeham, A., Correia, K.M., Samper, E., Brown, S., Aguilera, R.J., Nakano, T., Honjo, T., Mak, T.W., Rossant, J., et al. (1997). Conservation of the NOTCH signalling pathway in mammalian neurogenesis. Development *124*, 1139–1148.

Faul, F., Erdfelder, E., Lang, A.G., and Buchner, A. (2007). G*Power 3: a flexible statistical power analysis program for the social, behavioral, and biomedical sciences. Behav. Res. Methods *39*, 175–191.

Geling, A., Steiner, H., Willem, M., Bally-Cuif, L., and Haass, C. (2002). A gamma-secretase inhibitor blocks NOTCH signaling in vivo and causes a severe neurogenic phenotype in zebrafish. EMBO Rep. *3*, 688–694.

Hatakeyama, J., Bessho, Y., Katoh, K., Ookawara, S., Fujioka, M., Guillemot, F., and Kageyama, R. (2004). Hes genes regulate size, shape and histogenesis of the nervous system by control of the timing of neural stem cell differentiation. Development *131*, 5539–5550.

Imayoshi, I., Isomura, A., Harima, Y., Kawaguchi, K., Kori, H., Miyachi, H., Fujiwara, T., Ishidate, F., and Kageyama, R. (2013). Oscillatory control of factors determining multipotency and fate in mouse neural progenitors. Science *342*, 1203–1208.

Ishibashi, M., Ang, S.L., Shiota, K., Nakanishi, S., Kageyama, R., and Guillemot, F. (1995). Targeted disruption of mammalian hairy and Enhancer of split homolog-1 (HES-1) leads to up-regulation of neural helix-loop-helix factors, premature neurogenesis, and severe neural tube defects. Genes Dev. *9*, 3136–3148.

Iwahara, N., Hisahara, S., Hayashi, T., and Horio, Y. (2009). Transcriptional activation of NAD+-dependent protein deacetylase SIRT1 by nuclear receptor TLX. Biochem. Biophys. Res. Commun. *386*, 671–675.

Kawaguchi, D., Furutachi, S., Kawai, H., Hozumi, K., and Gotoh, Y. (2013). Dll1 maintains quiescence of adult neural stem cells and segregates asymmetrically during mitosis. Nat. Commun. *4*, 1880.

Kawai, H., Kawaguchi, D., Kuebrich, B.D., Kitamoto, T., Yamaguchi, M., Gotoh, Y., and Furutachi, S. (2017). Area-specific regulation of quiescent neural stem cells by NOTCH3 in the adult mouse subependymal zone. J. Neurosci. *37*, 11867–11880.

Khatri, P., Obernier, K., Simeonova, I.K., Hellwig, A., Holzl-Wenig, G., Mandl, C., Scholl, C., Wolfl, S., Winkler, J., Gaspar, J.A., et al. (2014). Proliferation and cilia dynamics in neural stem cells prospectively isolated from the SEZ. Sci. Rep. *4*, 3803.

Kobayashi, T., Mizuno, H., Imayoshi, I., Furusawa, C., Shirahige, K., and Kageyama, R. (2009). The cyclic gene Hes1 contributes to diverse differentiation responses of embryonic stem cells. Genes Dev. *23*, 1870–1875.

Li, S., Sun, G., Murai, K., Ye, P., and Shi, Y. (2012). Characterization of TLX expression in neural stem cells and progenitor cells in adult brains. PLoS One *7*, e43324.

Li, W., Sun, G., Yang, S., Qu, Q., Nakashima, K., and Shi, Y. (2008). Nuclear receptor TLX regulates cell cycle progression in neural stem cells of the developing brain. Mol. Endocrinol. *22*, 56–64.

Liu, H.K., Belz, T., Bock, D., Takacs, A., Wu, H., Lichter, P., Chai, M., and Schutz, G. (2008). The nuclear receptor tailless is required for neurogenesis in the adult subventricular zone. Genes Dev. *22*, 2473–2478.

Lois, C., Hong, E.J., Pease, S., Brown, E.J., and Baltimore, D. (2002). Germline transmission and tissue-specific expression of transgenes delivered by lentiviral vectors. Science *295*, 868–872.

Luque-Molina, I., Khatri, P., Schmidt-Edelkraut, U., Simeonova, I.K., Holzl-Wenig, G., Mandl, C., and Ciccolini, F. (2017). Bone morphogenetic protein promotes Lewis X stage-specific embryonic antigen 1 expression thereby interfering with neural precursor and stem cell proliferation. Stem Cells *35*, 2417–2429.

Lutolf, S., Radtke, F., Aguet, M., Suter, U., and Taylor, V. (2002). NOTCH1 is required for neuronal and glial differentiation in the cerebellum. Development *129*, 373–385.

Martynoga, B., Mateo, J.L., Zhou, B., Andersen, J., Achimastou, A., Urban, N., van den Berg, D., Georgopoulou, D., Hadjur, S., Wittbrodt, J., et al. (2013). Epigenomic enhancer annotation reveals a key role for NFIX in neural stem cell quiescence. Genes Dev. *27*, 1769–1786.

McKenzie, G., Ward, G., Stallwood, Y., Briend, E., Papadia, S., Lennard, A., Turner, M., Champion, B., and Hardingham, G.E. (2006). Cellular Notch responsiveness is defined by phosphoinositide 3-kinase-dependent signals. BMC Cell Biol. *7*, 10.

Monaghan, A.P., Bock, D., Gass, P., Schwager, A., Wolfer, D.P., Lipp, H.P., and Schutz, G. (1997). Defective limbic system in mice lacking the tailless gene. Nature *390*, 515–517.

Monaghan, A.P., Grau, E., Bock, D., and Schutz, G. (1995). The mouse homolog of the orphan nuclear receptor tailless is expressed in the developing forebrain. Development *121*, 839–853.

Nelson, B.R., Hodge, R.D., Bedogni, F., and Hevner, R.F. (2013). Dynamic interactions between intermediate neurogenic progenitors and radial glia in embryonic mouse neocortex: potential role in Dll1-NOTCH signaling. J. Neurosci. *33*, 9122–9139.

Nishimura, M., Isaka, F., Ishibashi, M., Tomita, K., Tsuda, H., Nakanishi, S., and Kageyama, R. (1998). Structure, chromosomal locus, and promoter of mouse *Hes2*Gene, a homologue of *Drosophila hairy* and *Enhancer of split*. Genomics *49*, 69–75.

Obernier, K., Cebrian-Silla, A., Thomson, M., Parraguez, J.I., Anderson, R., Guinto, C., Rodas Rodriguez, J., Garcia-Verdugo, J.M., and Alvarez-Buylla, A. (2018). Adult neurogenesis is sustained by symmetric self-renewal and differentiation. Cell Stem Cell *22*, 221–234.e8.

Obernier, K., Simeonova, I., Fila, T., Mandl, C., Holzl-Wenig, G., Monaghan-Nichols, P., and Ciccolini, F. (2011). Expression of Tlx in both stem cells and transit amplifying progenitors regulates stem cell activation and differentiation in the neonatal lateral subependymal zone. Stem Cells *29*, 1415–1426.

Ohtsuka, T., Ishibashi, M., Gradwohl, G., Nakanishi, S., Guillemot, F., and Kageyama, R. (1999). Hes1 and Hes5 as NOTCH effectors in mammalian neuronal differentiation. EMBO J. *18*, 2196–2207.

Pollard, S.M., Conti, L., Sun, Y., Goffredo, D., and Smith, A. (2006). Adherent neural stem (NS) cells from fetal and adult forebrain. Cereb. Cortex *16* (*Suppl 1*), i112–120.

Roy, K., Kuznicki, K., Wu, Q., Sun, Z., Bock, D., Schutz, G., Vranich, N., and Monaghan, A.P. (2004). The Tlx gene regulates the timing of neurogenesis in the cortex. J. Neurosci. *24*, 8333–8345.

Sepp, M., Pruunsild, P., and Timmusk, T. (2012). Pitt-Hopkins syndrome-associated mutations in TCF4 lead to variable impairment of the transcription factor function ranging from hypomorphic to dominant-negative effects. Hum. Mol. Genet. *21*, 2873–2888.

Shi, Y., Chichung Lie, D., Taupin, P., Nakashima, K., Ray, J., Yu, R.T., Gage, F.H., and Evans, R.M. (2004). Expression and function of orphan nuclear receptor TLX in adult neural stem cells. Nature *427*, 78–83.

Shitamukai, A., Konno, D., and Matsuzaki, F. (2011). Oblique radial glial divisions in the developing mouse neocortex induce self-renewing progenitors outside the germinal zone that resemble primate outer subventricular zone progenitors. J. Neurosci. *31*, 3683–3695.

Sueda, R., Imayoshi, I., Harima, Y., and Kageyama, R. (2019). High Hes1 expression and resultant Ascl1 suppression regulate quiescent vs. active neural stem cells in the adult mouse brain. Genes Dev. *33*, 511–523.

Sun, G., Yu, R.T., Evans, R.M., and Shi, Y. (2007). Orphan nuclear receptor TLX recruits histone deacetylases to repress transcription and regulate neural stem cell proliferation. Proc. Natl. Acad. Sci. U S A *104*, 15282–15287.

Sun, Y., Hu, J., Zhou, L., Pollard, S.M., and Smith, A. (2011). Interplay between FGF2 and BMP controls the self-renewal, dormancy and differentiation of rat neural stem cells. J. Cell Sci. *124*, 1867–1877.

VergHese, E., Schocken, J., Jacob, S., Wimer, A.M., Royce, R., Nesmith, J.E., Baer, G.M., Clever, S., McCain, E., Lakowski, B., et al. (2011). The tailless ortholog nhr-67 functions in the development of the *C. elegans* ventral uterus. Dev. Biol. *356*, 516–528.

Yu, R.T., McKeown, M., Evans, R.M., and Umesono, K. (1994). Relationship between *Drosophila* gap gene tailless and a vertebrate nuclear receptor Tlx. Nature *370*, 375–379.